Materials and Design 64 (2014) 631–639

Contents lists available at ScienceDirect

Materials and Design

journal homepage: www.elsevier.com/locate/matdes

Constitutive modeling of the thermo-mechanical fatigue and lifetime behavior of the cast steel 1.4849

F. Ohmenhäuser [a], C. Schwarz [b,*], S. Thalmair [a], H.S. Evirgen [a]

[a] BMW Group, 80788 München, Germany
[b] Lehrstuhl für Werkstoffkunde und Werkstoffmechanik, Technische Universität München, Boltzmannstr. 15, 85748 Garching, Germany

ARTICLE INFO

Article history:
Received 30 May 2014
Accepted 6 August 2014
Available online 19 August 2014

Keywords:
Austenitic cast steel
Cyclic properties
Low cycle fatigue
Fatigue modeling
Life prediction

ABSTRACT

A life prediction model for the austenitic steel 1.4849 is developed that can be integrated efficiently in the industrial product development process. The material is characterized by isothermal low-cycle-fatigue (LCF) and thermo-mechanical-fatigue (TMF) tests over a wide temperature range. A simple rheological constitutive model is adjusted to the experimental results, whereby special value is set on a physically reasonable and efficient reduction of the parameter set. The Manson–Coffin damage law is enhanced by a temperature dependent parameter in order to reproduce adequately the failure characteristics of the material. Application of the derived model in a thermo-mechanical simulation of a turbine housing illustrates its good quality: the predicted critical positions correlate well with the experimental results.

1. Introduction

1.1. Charging systems

A growing number of internal combustion engines rely on a charging system. Most widely used are turbo chargers, Fig. 1. One important objective which can be achieved by the use of turbo chargers is to downsize engines in order to reduce friction losses. Essential part of a turbo charger is the (centrifugal) compressor (left part in Fig. 1) which increases the mass of air entering the engine, thereby resulting in greater power and efficiency. The turbine (right part in Fig. 1) is driven by the exhaust gases of the engine, making use of a part of the otherwise lost energy of the exhaust gases.

The efficiency of engines strongly depends on the admissible maximum temperature of the exhaust gas, which in gasoline engines ranges from 850 to 1050 °C at the entrance of the turbine housing. The design of the exhaust gas system and especially the geometrically complex turbine housing are challenging tasks due to the wide range of occuring temperatures and the associated thermo-mechanical loads which have to be endured. The actual loads depend on the temperature of the exhaust gas, on cooling conditions due to thermal coupling to neighboring components, on the air flow around the engine, and on details such as wall thicknesses and local changes of stiffness.

The turbine housing is usually an austenitic steel casting. To account for the typical loading, the material needs high strength at elevated temperatures and high fracture elongation, which corresponds to good thermo-mechanical properties. Furthermore, adequate corrosion resistance is necessary at these high temperatures. These requirements are met by increasing the nickel content and the addition of carbon ligating metals such as titanium, tungsten or niobium. A typical quality for applications up to 980 °C is 1.4848 (HK-30, 18% Ni), for applications up to 1050 °C 1.4849 (HU-50, 36% Ni, 1.8% Nb), cf. Table 1 and [2]. If the requirements are not met with 1.4849 even Ni based alloys might be necessary. Since the material choice is very cost sensitive, the material is used to its limit.

In order to identify these limits with a minimum of costly and time-consuming experiments, computational lifetime prediction is becoming an important tool.

1.2. Lifetime prediction process

Four basic constituents of the lifetime prediction process for a thermo-mechanically loaded component are shown in Fig. 2.

1.2.1. Determination of the thermodynamical loading

The geometrically complex components in the hottest part of the exhaust gas system, e.g. the turbo charger, are stressed primarily through constrained thermal strains. Regular operation of internal combustion engines in cars implies cyclic changes of engine load from resting over idling, from small load up to full throttle.

* Corresponding author. Tel.: +49 89 289 15314.
E-mail address: schwarz@wkm.mw.tum.de (C. Schwarz).

http://dx.doi.org/10.1016/j.matdes.2014.08.016
0261-3069/

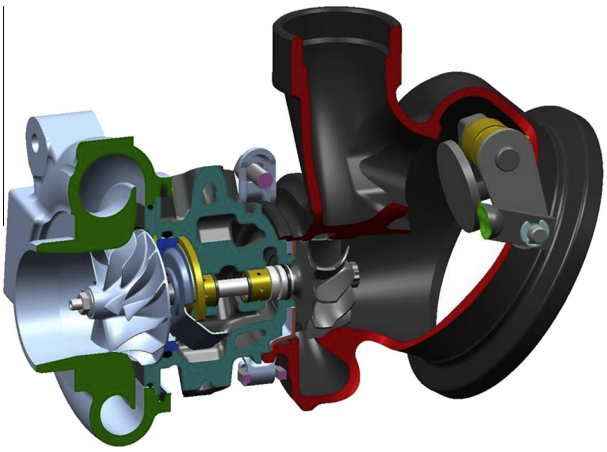

Fig. 1. Turbo charger (cross section), cf. [1].

These transient load variations lead to transient temperature distributions and thus thermal strains. The correct determination of the transient temperature field is critically important within the lifetime prediction procedure due to the twofold influence of the temperature, which is introducing thermal loads through thermal strains and determining the strongly temperature dependent constitutive behavior of the material.

Therefore much effort is put into the task of calculating the transient temperature distribution of the turbo charger with the best possible accuracy. This is however not a topic of the present contribution, rather is the transient temperature distribution taken as a given boundary condition.

1.2.2. Choice of constitutive model and damage criterion

Other critical constituents of the lifetime prediction procedure are related to the description of the material's behavior. In this contribution we focus on setting up an applicable constitutive model and on the relevant steps to implement the model into the lifetime prediction procedure, see also for example [3]. These are the highlighted parts in Fig. 2.

Thermal loading and constitutive material behavior determine the thermo-mechanical response of the examined structural component. The cyclic loading leads to a cyclic stress–strain history as response. Based on this response the lifetime can be predicted by means of a suitable lifetime criterion.

For the application in an industrial context the modeling procedure has to be integrable into the product development process. This means, the complexity of the constitutive material model and the resulting computational effort have to permit an analysis of a complex structure like a turbo charger within a reasonable time. Typically it is not possible to simulate a complete lifetime

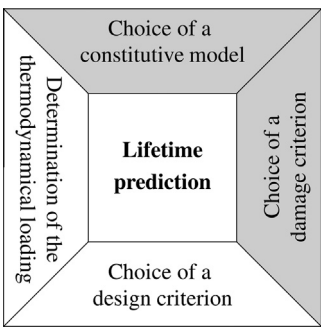

Fig. 2. Four basic constituents of the lifetime prediction process.

Table 1
Composition of the austenitic steel 1.4849.

Element	% C	% Ni	% Cr	% Nb
Content	0.3–0.5	36–39	18–21	1.2–1.8
% Si	% Mn	% Mo	% P	% S
1.0–2.5	⩽2.0	⩽0.5	⩽0.04	⩽0.03

with a structural finite element model using a continuum damage approach.

In structures operating at such high temperatures (i.e. above half the melting temperature of the material: $T_{op} > T_m/2$), the stress distribution after casting and assembling are mostly relaxed within the first few cycles. The actual stress distribution will then be driven by the thermo-mechanical load history, i.e. the transient temperature distribution. Thus, it is sufficient to evaluate a stabilized state of the material, which will be achieved after a small number of cycles [4,5]. These aspects guide the modeling approach presented in the main part of this work.

1.2.3. Design criterion

The fourth constituent of the lifetime prediction process is the choice of a suitable design criterion. The design criterion gives the necessary threshold for the damage criterion to ensure the integrity for a whole product life at the customer. As this is not within the scope of this paper, the following paragraphs will summarize only briefly a few important aspects of the design criterion with respect to the described application.

Criticality of cracks. Cracks emerge early in the lifetime of high temperature resistant stainless steel alloys under thermo-mechanical loading. Typically at about 10% of overall lifetime the first microcracks can be seen. Thus, to consider the achievable lifetime for a component, an allowable crack length has do be defined which can be considered macroscopic crack onset for typical applications.

For the examined cylindrical specimen with a diameter of 7 mm a crack length of 1 mm is considered as onset of a macroscopic crack. The measurable property during the lifetime experiments is the stiffness of the specimen. A stiffness loss of 10% is considered failure. Due to the rapid loss of stiffness after the onset of macroscopic cracks, this criterion is rather robust.

Operation mode and time. The number of cycles a component has to endure and the cycle amplitudes taken into account, can be taken from the analysis and a data extraction process of customers operating the considered component. The main result thereof is a dominant maximum load envelope in terms of minimum and maximum temperature and associated amplitude of mechanical strain. Accounting for the full engine life, the number of thermo-mechanical cycles with the full enveloping amplitude in the low-cycle-fatigue (LCF) regime typically are in the range of 10^3–10^4.

Component specifics. The continuum mechanics evaluation leads to a number of critical locations on an examined component. But not all potential cracks are created equally: on different locations, the propensity of a crack to propagate is different, the cross section which the crack has to pass through changes, and the load redistribution due to crack opening can vary, resulting in either reduced or accelerated crack growth. Here, engineering expertise and experience step in and help to further evaluate the results.

1.3. Scope of this contribution

The focus of this paper is set on modeling the material behavior of the austenitic steel 1.4849. A set of thermo-mechanical tests were carried out, which allow for the identification of the relevant

material properties within the operating temperature range from ambient conditions up to 1000 °C.

Section 2 describes the material and experimental data base. In Section 3 the constitutive modeling and the parameter identification procedures are shown, thereby watching applicability of the model within the FEM software ABAQUS [6]. In Section 4 we describe a suitable adaptation of the Manson–Coffin lifetime model. The so called 'integral approach' is discussed allowing for a conclusive intertwining of the modeling steps. Application of the defined model to a typical industrial example is shown in Section 5.

2. Material and experiments

2.1. Material

An iron base alloy which proved to be suitable for the application field at hand is the austenitic steel alloy 1.4849, featuring excellent behavior with regard to ductility, creep and oxidation resistance [2]. Its chemical composition is summarized in Table 1. The micrograph given in Fig. 3 reveals that the austenite solidified in a distinguished dendritic structure, inbetween which ferritic areas with small precipitates of δ-ferrite are present.

2.2. Experiments

In order to identify the material's behavior under thermo-mechanical loading, isothermal low-cycle-fatigue (LCF) and thermo-mechanical-fatigue (TMF) tests were conducted by the Fraunhofer Institute for Mechanics of Materials (IWM).

LCF tests at 8 temperatures were conducted, ranging from ambient condition up to 1000 °C. At each temperature two specimens were examined. A sophisticated strain controlled load history was applied, including a non-periodic part with high and low strain rates and holding times in tension and compression, and a periodic part as the actual fatigue test. Plasticity, the effects of rate dependence and stress relaxation can be measured by this type of experiment. Thus, a thorough basis is provided to identify the constitutive behavior.

Additionally, TMF tests in the temperature bounds of 200–950 °C were carried out under out-of-phase conditions. The specimens were cyclically heated and cooled, a cycle period took 500 s. The thermo-mechanical loading resulted from the total or partial constriction of the thermal elongation, resulting in compliances of 0%, 30% and 50%, respectively. Setup and procedure of the experiments have been published by the Fraunhofer IWM [7].

2.3. Characterization of the material's behavior

The various conducted tests show the viscoplastic behavior of the austenitic cast steel 1.4849 from ambient condition up to 1000 °C.

Ductility and monotonic hardening. A primary requirement for the examined alloy is ductile behavior over the complete temperature range. Apart from the cyclic tests, this can also be seen in the monotonically loaded hot tensile tests. The rupture strains (A_5) are approximately 10% from ambient condition up to 700 °C and larger than 20% for higher temperatures. Significant hardening can be seen in all tests up to 700 °C. In the tests at higher temperatures, the amount of hardening decreases with increasing temperature and the material behaves increasingly viscous. At these high temperatures, the achieved maximal stress is only meaningful in the context of the loading speed, i.e. the applied strain rate.

Viscous behavior. Another quality of highly thermo-mechanically resistant alloys can be seen in their temperature dependent viscous behavior. The steel 1.4849 exhibits only minor relaxation up to 600 °C. The tests at higher temperatures show increasing amounts of stress relaxation with increasing temperatures. As the material will be exposed to this temperature range, it is important to account adequately for the viscous behavior in the constitutive model.

Strain rate sensitivity. In conjunction with the viscous behavior, the type and amount of strain rate sensitivity has to be discussed. At ambient temperature and in the high temperature regime above 600 °C, the expected positive strain rate sensitivity can be observed: higher applied strain rates lead to higher stress variations. Consistent with the described viscous behavior in the high temperature regime, the strain rate sensitivity increases with the temperature.

In the intermediate temperature regime up to 600 °C, however, a different behavior can be observed, a *negative* strain rate sensitivity: increasing strain rates lead to lower stress variations.

Cyclic hardening and softening. In the same LCF tests, in which negative strain rate sensitivity has been observed, cyclic hardening occurs. This means, over the lifetime in the respective LCF tests, that the stress amplitude raises significantly as compared to the initial amplitude. At ambient condition, and again in the high temperature regime above 600 °C, the stress variation in the LCF tests remain nearly stable, only minor softening occurs.

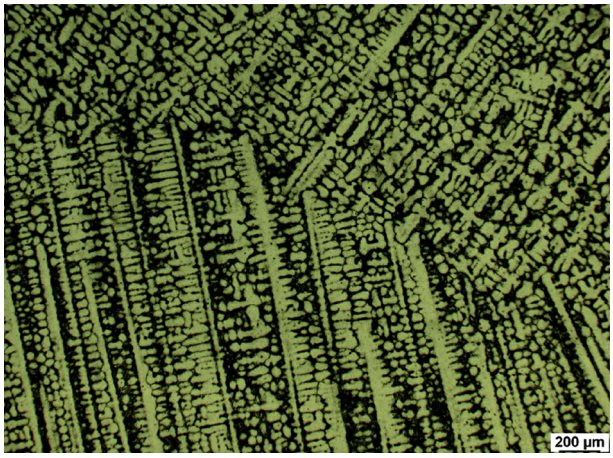

Fig. 3. Micrograph of the investigated material 1.4849. The austenite (light) solidified in a distinguished dendritic structure. Inbetween, ferritic areas (dark) with small precipitates of δ-ferrite are present, and pores can be observed. The material was prepared with V2A etchant.

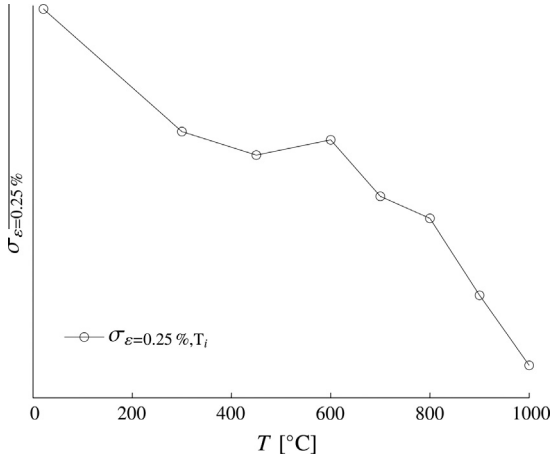

Fig. 4. Cyclic maximum stress at 0.25% strain amplitude vs. temperature: the non-monotonous shape of the curve indicates processes of dynamic strain ageing.

Table 2
Overview of temperature dependent nonlinear behavior. Remarkable entries are *emphasized*.

	Ambient condition	Intermediate temperature (up to 600 °C)	High temperature range
(Monotonic) Hardening	Significant	Significant	Decreasing with temperature
Relaxation	Minor	*Minor*	Moderate to significant; increasing with temperature
Strain rate sensitivity	Small positive	*Negative*	Positive; increasing with temperature
Cyclic behavior	Stable	Hardening	Minor softening

To give an impression of the temperature dependent cyclic behavior, the maximum cyclic stress at 0.25% strain amplitude measured in LCF tests over the whole temperature range is shown in Fig. 4. The expected monotonously decreasing stress over temperature is interupted by a plateau-like area with a distinguished rise at 600 °C. This is the temperature range with negative strain rate sensitivity and pronounced cyclic hardening.

An overview of the temperature dependent nonlinear behavior is given in Table 2.

Dynamic strain ageing. We assume, that the described behavior is caused by processes of dynamic strain ageing (DSA), also known as Portevin-Le Châtelier effect (PLC), which are due to the interactions of mobile dislocations with solute atoms resulting in a change of the dislocation glide mode [8,9]. In recent years, there have been extensive studies of such behavior in similar steel grades [10–12]. The serrated yielding, that is reported to be a typical implication, cannot be observed in the present experiments as the applied strain amplitudes are too small.

The observed effects suggest that the chosen constitutive model, cf. Section 3, will not be able to model the material's behavior consistently well in the whole temperature range, as cyclic changes are not incorporated.

3. Modeling of the constitutive behavior

In contrast to [7] where the focus is on fatigue life prediction based on a fracture mechanics model, the scope of this work is to identify parameters for suitable, simple constitutive and damage models that are able to represent the main features of the material behavior and that can at the same time be easily and efficiently used in standard FEM packages such as Abaqus.

3.1. Description

The two-layer viscoplastic constitutive model according to the rheological model outlined in Fig. 5 was chosen. It is appropriate for modeling materials that exhibit a significant viscoplastic behavior as it is typically displayed by metals at elevated temperatures. Its rheological representation consists of an elasto-plastic branch in parallel with an elasto-viscous branch.

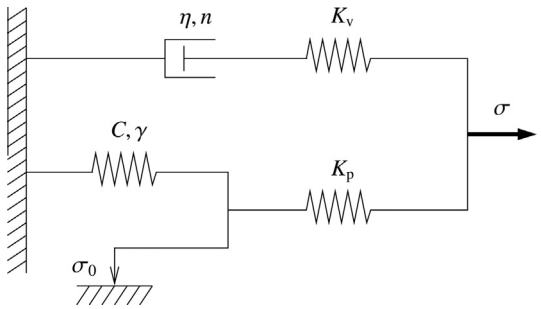

Fig. 5. Two-layer viscoplastic model, representation as rheological body.

The model was originally presented in the context of modeling polyethylene [13]. It has since been already very successfully employed for modeling the fatigue behavior of a gray cast iron [5] and an Al–Si-cast alloy [14,15].

A total Young's modulus E is defined as $E = K_p + K_v$, where K_p and K_v are the elastic moduli of the two branches of the model: the lower, plastic branch and the upper, viscous branch. Furthermore, the ratio f_v of the elasto-viscous network's modulus K_v and the total modulus E is introduced: $f_v = K_v/E$. The friction element controls the onset of plasticity in the model, related by the initial yield stress σ_0. The parameters C and γ describe the evolution of the back-stress q in the nonlinear kinematic hardening material model, isotropic hardening is not implemented. The viscous behavior is represented by the dash-pot in the upper branch. It is assumed to be governed by the Norton-Hoff rate law, $\dot{\varepsilon}_v = (\sigma_v/\eta)^n$, where η and n are Norton-Hoff rate parameters. The total stress σ is composed of the stresses in the viscous branch, σ_v, and in the plastic branch, σ_p, which are in turn related to the total strain ε, the viscous strain ε_v of the dash-pot and the plastic strain ε_p of the friction element, respectively. The resulting set of constitutive equations, compare [14], results for the one-dimensional case as:

$$
\begin{aligned}
&f(\sigma, q) = |\sigma - q| - \sigma_0 && \text{(yield function)}\\
&\dot{q} = C\dot{\varepsilon}_p - \gamma q|\dot{\varepsilon}_p| && \text{(back stress rate)}\\
&\dot{\varepsilon}_p = |\dot{\varepsilon}_p|\operatorname{sgn}(\sigma_p - q) && \text{(plastic strain rate)}\\
&\dot{\varepsilon}_v = \left(\frac{\sigma_v}{\eta}\right)^n \operatorname{sgn}(\sigma_v) && \text{(viscous strain rate)}\\
&\sigma_p = K_p(\varepsilon - \varepsilon_p)\\
&\sigma_v = K_v(\varepsilon - \varepsilon_v)\\
&\sigma = \sigma_p + \sigma_v
\end{aligned}
\qquad (1)
$$

3.2. Discussion

The simple model chosen accounts for the following significant phenomena which are observed in the experiments.

The Bauschinger effect is characterized by a reduced yield stress upon load reversal after plastic deformation has occured during the initial loading. This phenomenon decreases with continued cycling.

Cyclic hardening with plastic shakedown is characteristic of symmetric stress- or strain-controlled experiments. Metals tend to harden toward a stable limit.

Relaxation at high temperatures is accounted for in the viscous branch. However, it is required to pay attention to the following: Including only a kinematic hardening component in the model, plastic shakedown is predicted already after one stress cycle. The combination with an isotropic hardening component would predict shakedown after several cycles only, which matches better with the experimental data. Therefore, a perfect agreement of the model and the experiments cannot be expected. Being aware of this problem, and as the objective of most industrial applications is a representation of the stabilized cycle for the following lifetime approximation [16], the parameter identification is based on the stress–strain-behavior one finds after a sufficiently large number of load cycles.

3.3. Parameter identification

The identification of the model parameters introduced along with Fig. 5 was performed on the basis of the non-periodic parts of the LCF tests only, cf. Section 2.2, and was realized in two steps.

3.3.1. Parameters for isothermal LCF tests

In a first step, for each of the 16 isothermal LCF tests an individual set of parameters was determined. The optimization is conducted on the basis of a Covariance Matrix Adaptation Evolution Strategy (CMA-ES) [17,18]. This is an evolutionary algorithm for demanding non-linear non-convex optimization problems in continuous domains which is typically applied to unconstrained or bounded constraint optimization problems and which copes very well with the existence of local minima. The objective of the optimization is to minimize the least squares (LSQ) function:

$$\mathrm{LSQ} = \frac{1}{N}\sum_{i=1}^{N}\left(\sigma_i^{\mathrm{mod}} - \sigma_i^{\mathrm{meas}}\right)^2. \tag{2}$$

For N data points, σ_i^{meas} represents the stress measured in the respective experiment at data point i, and σ_i^{mod} is the corresponding stress value predicted by the model on the basis of the given strain and strain rate and the current set of model parameters.

Relaxation takes place during the holding times of the load path. As the data registered during the experiments are uniformly distributed over time, one must take care that these data segments do not rule the parameter optimization by their pure dominance of the number of data points. This is accomplished by calculating the LSQ function as arithmetic mean of six LSQ functions determined in turn for subsets of the data corresponding to sections of the load history exhibiting uniform strain rate.

An example for the result of an isothermal optimization of a LCF experiment can be seen in Fig. 6. With this type of individual optimization, for each experiment (i.e. two per temperature) a parameter set can be found, that describes the constitutive behavior very well.

3.3.2. Temperature dependence of parameters

In a second step a simple function is used to describe the temperature dependence of *each* parameter. In the following, we discuss as an exemplification the results for one specific parameter. Fig. 7 shows the discrete parameter values and the regression function for the viscous parameter f_v. As can be seen a quadratic function adequately describes the temperature dependence of this parameter. This reduces the number of parameters that have to be optimized significantly. Instead of one parameter set for each temperature point, only the coefficients of the parameters' regression functions with respect to temperature and thus significantly less parameters are necessary to account for the temperature dependence.

As can be seen in Fig. 7, the parameter values determined in different tests at one temperature vary significantly. This is for the most part due to scatter in the material properties between the different specimens. Accuracy above this level of scatter does not improve the effective adaptation quality and is therefore not pursued.

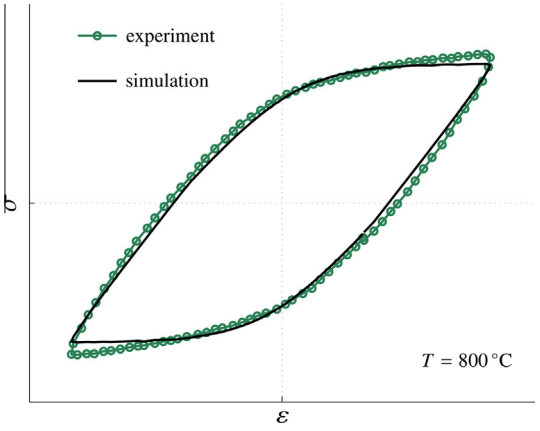

Fig. 6. Comparison of experimental and simulated hysteresis, LCF experiment at 800 °C.

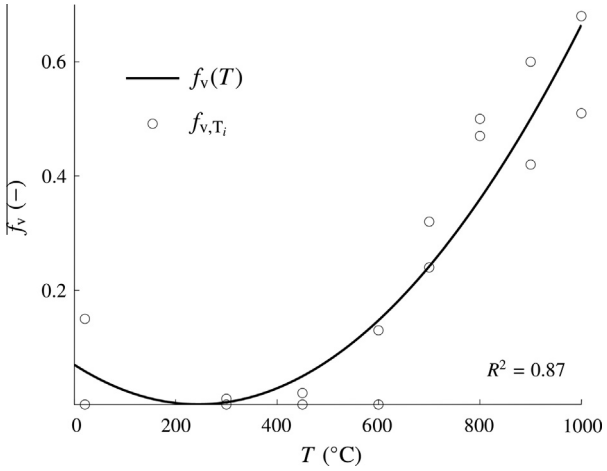

Fig. 7. Temperature dependence of the model parameter f_v and corresponding regression function $f_v(T)$.

The constitutive model has been chosen for its ability to model the described phenomena adequately. The experiments available were chosen such as to mimic the typical loads identified in structural components – not primarily to determine all constitutive parameters in the broadest possible range. For the time-dependent properties in the viscous part, this means that a rather narrow band of strain rate has been covered. Within this range, the viscosity parameters n and η are dependent on each other. Therefore, n was set to a value of 4, the standard Norton exponent for austenitic steels [19], and only η was determined through the optimization procedure.

As the computational cost rises significantly for each additional parameter which has to be determined, much time and effort has been put into the choice of the respective parameter-temperature-functions. Apart from the fixed parameter n, η has been set to be constant, and the only temperature dependent viscosity parameter has been the above described parameter f_v, the fraction of the viscous branch within the two-layer viscoplastic model.

Overall, this lead to a total number of 13 parameters for a temperature dependent representation of the seven variables $(E, f_v, \sigma_0, C, \gamma, \eta, n)$ that describe the constitutive behavior of the 1.4849 austenitic cast steel reasonably well.

3.4. Application of the constitutive model to a TMF test

The parameter set of the two-layer-viscoplastic model is assessed by comparing for non-isothermal TMF experiments the experimental results to the hysteresis curves simulated with the presented material model using the temperature dependent parameters determined on the basis of the LCF tests. Figs. 8 and 9 show a typical outcome.

On the whole, the characteristics of the simulated TMF experiment match the actual experimental result very well. The most obvious discrepancy is observed in the initial loading, which is however of minor relevance for the overall evaluation process and therefore considered to be acceptable.

In order to assess the differences between simulation and experiment properly, it has to be pointed out that the TMF experiments have not been used to derive the constitutive parameters. As discussed in Section 2.3, the cyclic changes of the examined steel are very different at different temperatures, whereas the

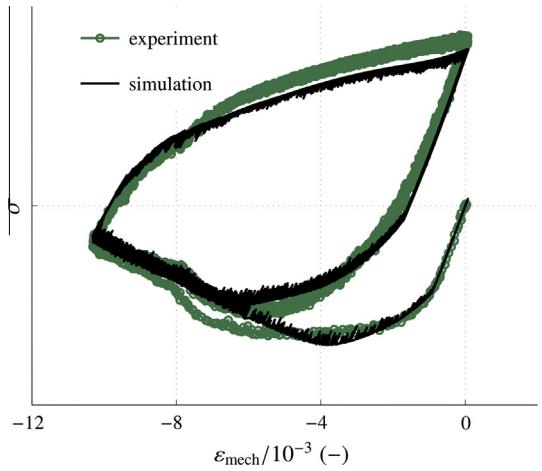

Fig. 8. Comparison of experimental and simulated hysteresis, TMF experiment between 200 and 950 °C with 30% compliance admitted. For better visibility, only every 5th experimental data point of the depicted nine complete cycles is plotted.

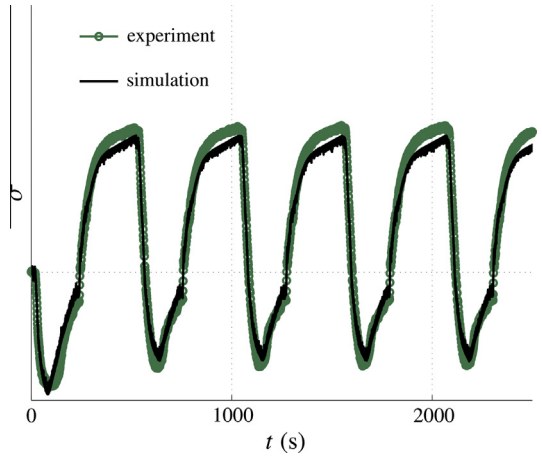

Fig. 9. Comparison of computed and simulated stress over time, TMF experiment between 200 and 950 °C with 30% compliance admitted. For better visibility, only every 5th experimental data point of the first four complete cycles corresponding to Fig. 8 is plotted.

constitutive parameters have been derived in order to achieve the best match for all LCF tests simultaneously, cf. Section 3.3. Moreover, the parameter identification procedure showed a significant amount of scatter between individual experiments, exemplified for the constitutive parameter f_v in Fig. 6.

Taking this ambiguity into account, the inelastic behavior of the material as assessed in non-isothermal TMF tests is remarkably well represented with the chosen constitutive model and the derived parameter set. The good prediction of TMF tests also indicates a good predicting capability of the model for the deformation and respective strain distribution in structural components.

4. Damage criterion

TMF lifetime in cast austenitic steels is mainly influenced by the accumulation of damage due to cyclic plastic deformation. A critical plane-energy based damage parameter is applied to the fatigue life assessment of engineering components in [20]. In [7] a fracture mechanics based lifetime prediction method for exhaust systems is presented. However, for the efficient use in the development process a simpler phenomenological law is preferable.

4.1. Simple Manson–Coffin law

The simple Manson–Coffin law describes that the number of cycles until failure N_f is inversely proportional to a positive power of the plastic strain amplitude per cycle [21–24]. In terms of a general independent damage measure P_{MC}, it is known in the form

$$N_f = a \cdot P_{MC}^{-b}, \quad \text{with } P_{MC} = \varepsilon_{pl,a}, \tag{3}$$

where a is a proportionality constant, $-b$ is the exponent and $\varepsilon_{pl,a}$ is the plastic strain amplitude. As in the present constitutive model, cf. Section 3.1, a plastic and a viscous strain are distinguished, a clearer notation bases on the quantity of an inelastic strain amplitude $\varepsilon_{in,a}$, which is composed of plastic and viscous contributions according to the applied constitutive model, Section 3.1:

$$N_f = a \cdot P_{MC}^{-b}, \quad \text{with } P_{MC} = \varepsilon_{in,a}, \tag{4}$$

Lifetime respectively fatigue limits are highly statistical quantities [8]. Assuming a Gaussian distribution of $\log N_f$, a statistical analysis of the experimental lifetimes determined within the LCF experiments at the different temperatures is performed. For visualization, linear curves indicating the limits of 10%, 50% and 90% failure probability p are plotted. A scatter band factor $s_{10\%/90\%}$ is given, defined as the ratio of the predicted lifetimes $N_{f,p=90\%}$ and $N_{f,p=10\%}$ for a fixed value of P_{MC}. The statistical coefficient of determination $R^2 \in [0;1]$ provides a measure for the reliability of the model prognosis. A value close to 1 suggests a very good model quality.

In the simple form given in Eq. (4), the Manson–Coffin law is not able to describe the temperature influence on lifetime adequately, Fig. 10. Here a common statistical analysis of all LCF data was performed.

4.2. Enhanced Manson–Coffin law

However, when LCF tests for only one temperature (or a set of similar temperatures) were considered for the statistical analysis, much narrower scatter bands result. Therefore, an enhanced formulation of the Manson–Coffin law involving a normalizing function $d(T)$ is introduced. By choosing a different, temperature dependent definition of the damage measure, $P_{MC}(T)$, a temperature corrected Manson–Coffin criterion is defined as

$$N_f = a \cdot P_{MC}(T)^{-b}, \quad \text{with } P_{MC}(T) = \frac{\varepsilon_{in,a}}{\sqrt[b]{d(T)}}. \tag{5}$$

The parameters for the proposed lifetime model are identified in a two-step procedure based firstly only on the LCF data. In the first

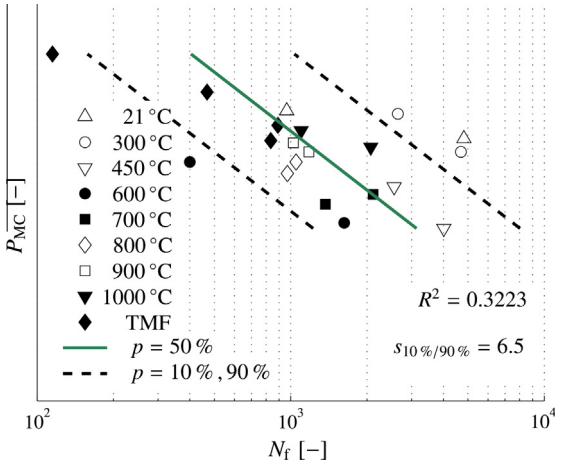

Fig. 10. Statistical analysis based on the simple Manson–Coffin law.

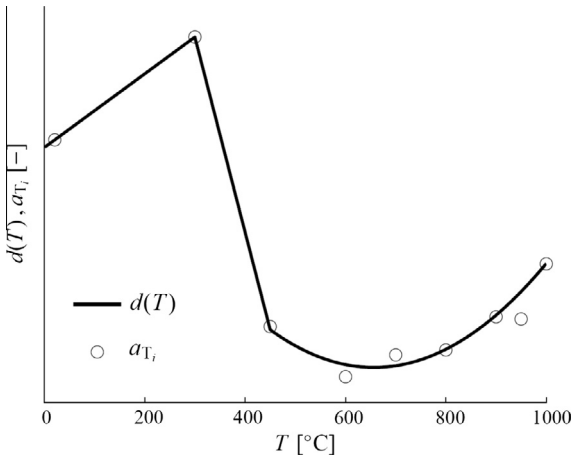

Fig. 11. Normalizing function $d(T)$ for the enhanced Manson–Coffin law.

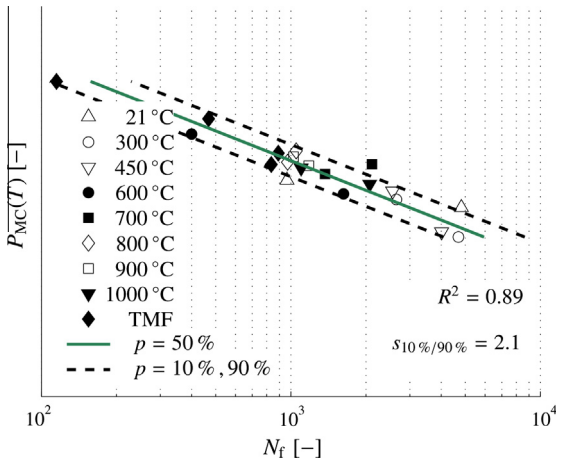

Fig. 12. Statistical analysis based on the enhanced Manson–Coffin law and including the TMF data.

step, the values of the constant a in Eq. (4) are determined for each temperature T_i assuming an estimated, identical value of the exponent $-b = -1.7$. The normalizing function $d(T)$ is determined as a suitable regression function of these individual values a_{T_i}. The chosen function, cf. Fig. 11, depends on five independent parameters that have to be determined. As there is little ambiguity between these parameter, not much effort has been spent to further reduce the number of parameters in the description of $d(T)$.

In the second step, the parameters a and $-b$ in Eq. (5) are determined from a statistical analysis involving all LCF data plus data provided by the conducted TMF tests. To choose the temperature value associated with the TMF tests, theoretical and practical aspects have been considered. From a theoretical point of view, a weighted average temperature seems reasonable. A more practical approach is to simply use the maximum temperature within the TMF cycle. Better values for both the correlation coefficient R^2 and the width of the scatter band $s_{10\%/90\%}$ were achieved on the basis of the practical approach. Results of the statistical analysis based on the enhanced Manson–Coffin law and involving the TMF data are displayed in Fig. 12.

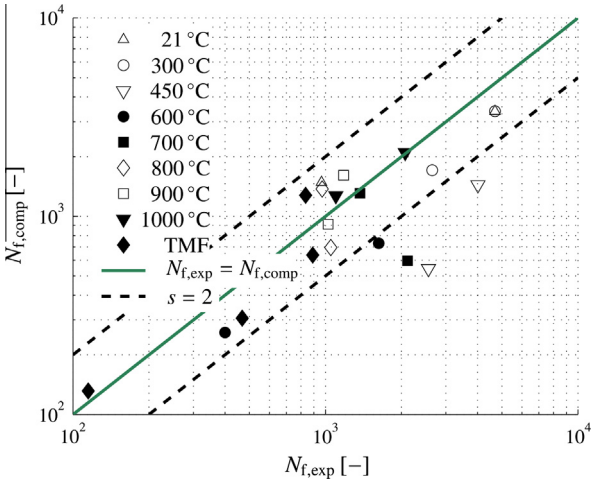

Fig. 13. Comparison between experimental and computed lifetimes. The dashed lines mark the scatter band of width $s = 2$.

4.3. Integral approach

In Section 3, the chosen two-layer visco-plastic constitutive model has been adapted to the described LCF tests and a reasonably good fit even to TMF tests has been shown. In this section, the parameters of an enhanced formulation of the Manson–Coffin law have been adapted to fit the results of all LCF and TMF tests. It has to be pointed out that this adaptation has been done on actual test results, i.e. the plastic strain amplitudes of the tests have been evaluated, resulting in the 'experimental lifetime' $N_{f,exp}$. However, the strain amplitudes of the respective tests might turn out differently when the tests are simulated using the adapted constitutive model. This last step is necessary to fully integrate the lifetime model into the lifetime prediction procedure, which is applicable to structural components in an industrial product development process.

The 'computed lifetimes' $N_{f,comp}$ are based on plastic strain amplitudes, computed with the chosen constitutive model and the load history of the respective LCF or TMF test, and the lifetime model parameters as determined in Section 4.2. Fig. 13 shows a comparison between the experimental and the computed lifetimes.

The agreement for four of the six LCF tests in the temperature range of 450 to 700 °C is unsatisfactory. In these LCF tests the most pronounced cyclic hardening occured. Therefore, this outcome may be due to the chosen material model which does not account for cyclic changes. Only one specified material state with respect to cyclic changes is taken as a basis for the adaptation of the model parameters. Here, the parameters have been determined such that the constitutive behavior best fits all performed LCF tests simultaneously, cf. Section 3.3.2. As the majority of the tests exhibit only small cyclic changes, the tests with pronounced cyclic hardening are not represented well by the chosen parameter set, respectively. However, as described in Section 1.2.2, in an industrial product development process only a few cycles (3–5) can be computed for the structural model of a component. Thus, even a constitutive model accounting for cyclic changes would not countervail this problem effectively. As to practical purposes, for the examined cast steel, damage occuring only in this temperature range is of secondary importance, and the experimental lifetime for these outstanding tests is higher than the computed, thus the prediction is conservative.

5. Application example

In this section, results from a typical application of the presented material model are shown: results of the thermo-mechanical simulation of the tongue region of the turbine housing as a typical region at risk, Fig. 14.

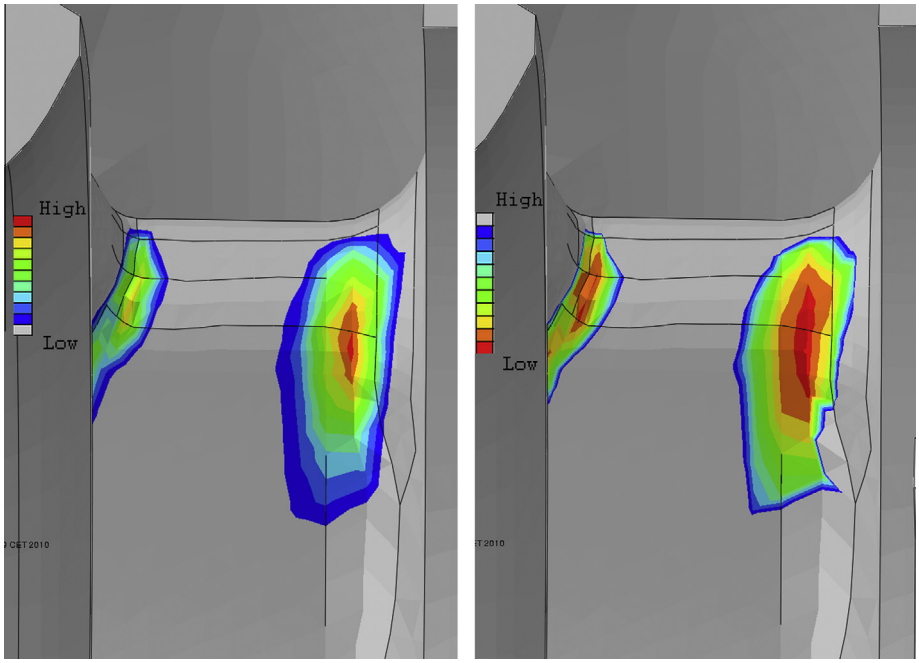

Fig. 14. Example result, tongue area of turbine housing: plastic strain amplitude (left) and cycles to macroscopic crack (right).

As described in Section 1.2.1, the primary load is due to the transient temperature distribution within the component examined. This temperature distribution is computed in a separate heat transfer analysis. Both, absolute values and the transient course of the temperature have to be carefully matched with the component on the test rig in order to achieve adequate predicting capabilities in the following thermo-mechanical finite element analysis (FEA) and lifetime prediction. Further boundary conditions considered are the constraints due to mounting and assembly of the component on the test rig and on the engine.

5.1. Details of the finite element analysis

The presented material model consists of a constitutive and a damage model. The constitutive model has been chosen such that it can be directly used in Abaqus [6].

To achieve a stabilized strain distribution consistent with the constitutive model, three to five cycles of the examined test sequence are ideally computed in the FEA. In a following post processing step, the amplitudes of the last cycle are evaluated and the respective lifetime is computed. Here, a Python [25] tool is used to efficiently compute the lifetime according to the chosen damage model. Effectively, the lifetime is available like other field variables to be visualized in the Abaqus Viewer or other common FEA post processors.

5.2. Results

In Fig. 14 results are shown for the tongue region of the turbine housing. The plot on the left shows the plastic strain amplitudes for the third computed load cycle. On the right, the subsequently computed lifetime is shown. In Fig. 15 the scroll region of the examined turbine housing is shown, the tongue laying on the right.

Qualitatively, results from the test rig correlate well with the predicted critical positions. As these crack positions typically do not lead to component failure, they are well suited also to evaluate them quantitatively. One has to bear in mind, that failure according to the proposed damage model means onset of a macroscopic crack, but not necessarily a crack through the whole wall. Therefore, repeated examination of the component at various fractions of the predicted lifetime could quite well confirm the prediction quantitatively, too. Such a detailed experimental examination was only possible, because the critical position was accessible through an endoscope without completely unmounting the test rig.

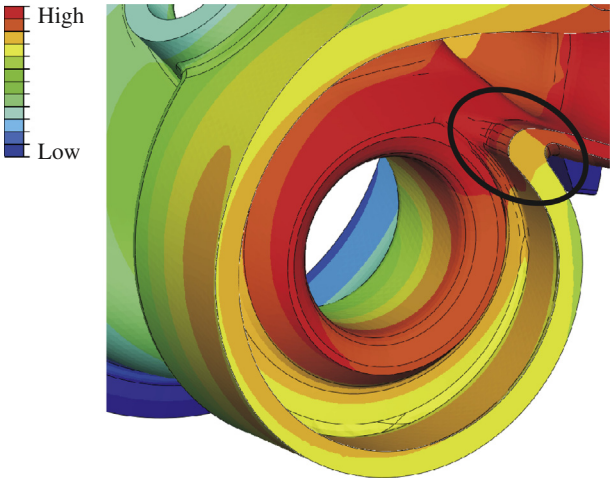

Fig. 15. Cross section of the examined turbine housing, scroll region; temperature distribution during transient heating. The black ellipse marks the critical tongue region, cf. Fig. 14.

5.3. Discussion

Most of the crack positions have been successfully predicted in the presented example FEM analysis of a turbine housing. As the focus in this paper is on the applied material model, other crack positions which have not been predicted adequately, and predicted critical areas without visible damage after the rig test will not be

discussed here. In the case of the two critical positions that were correctly identified, it has been possible to pin down the onset of macroscopic cracks rather well along the component test. Moreover, the crack propagation, the crack path and the eventual stopping of the crack were comprehensible. As a crack opens on one of the two positions, which lie quite close, the neighboring position will become less critical due to load redistribution.

Still, the presented material model allows for the prediction of crack onset only. In order to assess the effects of crack propagation and load redistribution, engineering expertise has to step in to further evaluate the results of the FEM analysis.

However, as in the future thermal loads will increase further whereas mechanical properties of the available cast alloys will not change significantly, certain cracks have to be allowed within current turbocharger design types and production capabilities. Engineering expertise alone might not be enough to successfully develop turbine housings that tolerate dependably cracks complying with certain safety restrictions imposed for example on their length and path. Therefor, more extensive and detailed simulations will be necessary.

The simulation of (mixed-mode) crack propagation using FEM is cumbersome though, as in classical approaches, e.g. [26], a repeated reconfiguration of the mesh is required in order to account for the altering geometry of the discontinuity. Several possible strategies to reduce the computational effort exist [27–29] and are examined. One of them is the extended finite element method (X-FEM) [27,28], which is also available in Abaqus [6].[1] It offers crack propagation without repeated remeshing. However, to the authors' knowledge, no application of this method to more intricate problems involving a three-dimensional simulation domain of complex geometry, a (visco-) plastic material behavior and cyclic crack propagation has been presented up to now.

6. Conclusions

For the austenitic cast steel alloy 1.4849, an extensive set of experiments have been carried out to characterize its constitutive and lifetime behavior under cyclic thermo-mechanical loads in the range of ambient temperature up to 1000 °C. It has been shown that the chosen two-layer viscoplastic constitutive model can be well adapted to the measured behavior from the specimen experiments. Along with the strategy to adapt the model parameters with respect to an optimal fit to all performed LCF tests simultaneously, special value has been set on a physically reasonable and efficient reduction of the parameter set. This could be accomplished by identifying simple temperature dependencies for the constitutive model parameters, which could be specified by a small parameter set. Application of the model to TMF experiments showed very good agreement of simulation and experiment, confirming its predictive capabilities and thereby the reasonableness of the chosen approach.

The Manson–Coffin damage law was taken as a basis for the lifetime model. Good results, manifesting themselves in narrow scatter bands for all experiments, were achieved by enhancing the model with a temperature dependent parameter that accounts for the altering material behavior.

Applying the presented model in a thermo-mechanical simulation of a typical region at risk of a turbine housing, it has eventually been shown how it can be incorporated into the CAE process for high temperature fatigue assessment of turbo chargers at BMW. The comparison of simulation results to engine and component tests show the good predictive capabilities of the evaluation process.

[1] http://www.simulia.com/download/rum11/UK/Advanced-XFEM-Analysis.pdf.

Acknowledgement

The authors would like to express their gratitude to Dr.-Ing. Wüchner, Chair of Structural Analysis at the Technische Universität München, for valuable discussions within this project.

Furthermore, the authors would also like to acknowledge BMW Group for the funding of this project and for the permission to publish the present contribution.

References

[1] Welter A, Bruener T, Unger H, Hoyer U, Brendel U. Der neue aufgeladene Reihensechszylinder-Ottomotor von BMW. MTZ – Motortech Zeitschrift 2007;68(2):80–9.
[2] Tliouant R. Hitzebeständiger Stahlguss GX40NiCrSiNb38-19 (Nr. 1.4849). Werkstoffdatenblatt; 2007.
[3] Kocabicak U, Firat M. A simple approach for multiaxial fatigue damage prediction based on FEM post-processing. Mater Des 2004;25:73–82.
[4] Constantinescu A, Van KD, Maitournam MH. A unified approach of low and high cycle fatigue based on a shakedown concept. Fatigue Fract Eng Mater Struct 2003;26:561–8.
[5] Charkaluk E, Bignonnet A, Constantinescu A, Van KD. Fatigue design of structures under thermomechanical loadings. Fatigue Fract Eng Mater Struct 2002;25:1199–206.
[6] Abaqus 6.10 analysis user's manual. Simulia; 2010.
[7] Seifert T, Schweizer C, Schlesinger M, Möser M, Eibl M. Thermomechanical fatigue of 1.4849 cast steel – experiments and life prediction using a fracture mechanics approach. Int J Mater Res 2010;101(8):942–50.
[8] Dieter GE. Mechanical metallurgy. McGraw-Hill Book Company; 1988.
[9] Zauter R, Petry F, Christ HJ, Mughrabi H. Thermomechanical fatigue of the austenitic stainless steel AISI 304 L. In: Sehitoglu H, editor. Thermomechanical fatigue behavior of materials, ASTM STP 1186, vol. 1. Philadelphia: American Society for Testing and Materials; 1993. p. 70–90.
[10] Nikulin I, Kaibyshev R, Skorobogatykh V. High temperature properties of an austenitic stainless steel. In: Proceedings of the 15th international conference on the strength of materials. Journal of physics: conference series (ICSMA), vol. 240; 2010. p. 012071.
[11] Peng K, Qian K, Chen W. Effect of dynamic strain aging on high temperature properties of austenitic stainless steel. Mater Sci Eng A 2004;379:372–7.
[12] Hector L, Zavattieri P. Nucleation and propagation of Portevin-Le Châtelier bands in austenitic steel with twinning induced plasticity. In: Proceedings of the SEM Annual Conference. SEM: Society for Experimental Mechanics Inc.; 2010.
[13] Kichenin J. Comportement thermomécanique du polyéthyléne. Application aux structures gaziéres. Ph.D. thesis, École polytechnique, Palaiseau, France; 1992.
[14] Thalmair S, Thiele J, Fischersworring-Bunk A, Ehart R, Guillou M. Cylinder heads for high power gasoline engines – thermomechanical fatigue life prediction. In: Fatigue research and applications. Detroit, MI, USA: SAE World Congress; 2006. SAE technical paper 2006-01-0541.
[15] Thalmair S. Thermomechanische Ermüdung von Aluminium-Silizium-Gusslegierungen unter ottomotorischer Beanspruchung. PhD thesis, Universität Karlsruhe; 2009.
[16] Constantinescu A, Charkaluk E, Lederer G, Verger L. A computational approach to thermomechanical fatigue. Int J Fatigue 2004;26:805–18.
[17] Hansen N, Müller SD, Koumoutsakos P. Reducing the time complexity of the derandomized evolution strategy with covariance matrix adaptation (CMA-ES). Evolution Comput 2003;11(1):1–18.
[18] Rechenberg I. EvoC 2.0 user manual. Technische Universität Berlin, Department of Bionics and Evolution Techniques; 1994.
[19] Suresh S. Fatigue of materials. Cambridge University Press; 1998.
[20] Varvani-Farahani A, Kianoush MR, Sharma M. Fatigue failure assessment of engineering components under service loading conditions. Mater Des 2007;28:575–80.
[21] Lemaitre J, Chaboche JL. Mechanics of solid materials. Cambridge University Press; 1990.
[22] Manson SS. Behavior of materials under condidtions of thermal stress. Tech. rep. 1170, NACA; 1954.
[23] Coffin LF. A study of the effects of cyclic thermal stresses on a ductile metal. Trans ASME 1954;76:931–50.
[24] Manson SS, Hirschberg MH. Fatigue behavior in strain cycling in the low and intermediate cycle range. In: 10th Sagamore army materials research conference; 1963.
[25] Python; 2014. <http://www.python.org/> [last visited 31/07/14].
[26] Swenson DV, Ingraffea AR. Modeling mixed-mode dynamic crack propagation using finite elements: theory and applications. Comput Mech 1988;3:381–97.
[27] Moës N, Dolbow J, Belytschko T. A finite element method for crack growth without remeshing. Int J Numer Methods Eng 1999;46(1):131–50.
[28] Song JH, Wang H, Belytschko T. A comparative study on finite element methods for dynamic fracture. Comput Mech 2008;42(2):239–50.
[29] Citarella R, Cricrí G, Lepore M, Perrella M. Thermo-mechanical crack propagation in aircraft engine vane by coupled fem-dbem approach. Adv Eng Softw 2014;67:57–69.